

Full Length Article

Investigation of corrosion mechanism in Type 304 stainless steel under different corrosive environments: A SIMS study



V. Karki*, M. Singh

Fuel Chemistry Division, Bhabha Atomic Research Centre, Mumbai, 400 085, India

ARTICLE INFO

Article history:

Received 19 April 2017

Received in revised form 31 May 2017

Accepted 3 June 2017

Available online 9 June 2017

Keywords:

SIMS

Investigation of corrosion using SIMS

Pitting corrosion

Austenitic stainless steel

Imaging

Depth distribution

Mass spectrum

ABSTRACT

Surface imaging, depth distribution and mass spectra analysis features of Secondary Ion Mass Spectrometry has been utilized for investigating the corrosion mechanism in Type 304 austenitic stainless steel under different corrosive environments of H_2SO_4 , HCl and HNO_3 solutions of 10 M each. Surface distribution analysis revealed non-homogenous distribution of alloying elements S, Cr, Mn, Ni and Fe in case of H_2SO_4 and HCl treated samples, which was due to the formation of corroded layer and its morphology. Depth distribution and mass spectra analysis revealed that oxides and hydroxides containing species are most abundant in H_2SO_4 treated sample followed by HCl treated sample. Surface distribution and mass spectra analysis indicated localized attack or pitting corrosion of chloride species in case of HCl treated specimen whereas in case of H_2SO_4 treated sample, attack of sulfur species was associated with an intensification of oxide and hydroxide species. Depth distribution analysis in case of HNO_3 treated specimen concluded the formation of a passive layer enriched with Cr, Ni, Mn and Fe which causes the inhibition of corrosion process under the experimental corrosive parameters. The study also provides a methodology to investigate the type of chemical attack and to find out the root cause of corrosion utilizing various analysis features of SIMS technique.

© 2017 Elsevier B.V. All rights reserved.

1. Introduction

Stainless steel is one of the most widely used construction material in the modern industrial regime [1]. Among different categories of stainless steel, austenitic stainless steel alloys are of great interest in technological applications where materials with high corrosion resistance are required. Owing to this property, austenitic stainless steels are used frequently as construction materials in aggressive environments such as nuclear industry [1,2], chemical plants [1], biomedical implants [3], fixations in civil engineering [1], etc. Moreover, austenitic stainless steels like AISI 304, AISI 316, etc., have been used in the nuclear industry (light water reactors (LWR) and fast breeder reactors (FBR)) [1]. Besides fission systems, these stainless steels are also regarded as a potentially suitable material for fusion systems [2]. Their generally excellent corrosion resistance is due to the spontaneous formation of a protective film with a thickness of order of few nanometres (1–4 nm) on the surface [4]. However, the behaviour of the passive film is determined by the alloy composition as well as the environmental conditions which such stainless steel is exposed to.

Extensive research has been carried out to understand the corrosion mechanism in steel and stainless steel alloys under different corrosive acidic environments by using chemical and electrochemical methods [1]. For instance Noor and Moubaraki investigated the corrosion behaviour and mechanism for mild steel in HCl solutions employing chemical and electrochemical methods. They observed that the mild steel corrodes in HCl solutions and the corrosion rate increases with increased acid concentration. They also observed a change in surface microstructure which was due to the pitting corrosion process [5]. Iliyasu et al. studied the corrosion mechanism of Type 304 austenitic stainless steel under different concentrations (0.3–1 M) of H_2SO_4 at ambient as well as at higher temperatures. They found that the steel was highly resistant to uniform corrosion in these environments but still susceptible to Stress Corrosion Cracking. They also observed that the corrosion rate increases with increase in temperature [6].

The chemical and electrochemical methods are laboratory based investigation techniques, primarily used for understanding the corrosion mechanism and corrosion rate in various materials under known corrosive environments. These investigations provide information about the behaviour of material in various environments. But in case of already corroded material in an unknown environment, various other surface and depth sensitive techniques like Secondary Ion Mass Spectrometer (SIMS), Scanning Electron

* Corresponding author.

E-mail addresses: vkarki@barc.gov.in, vijaykarki.karki@gmail.com (V. Karki).

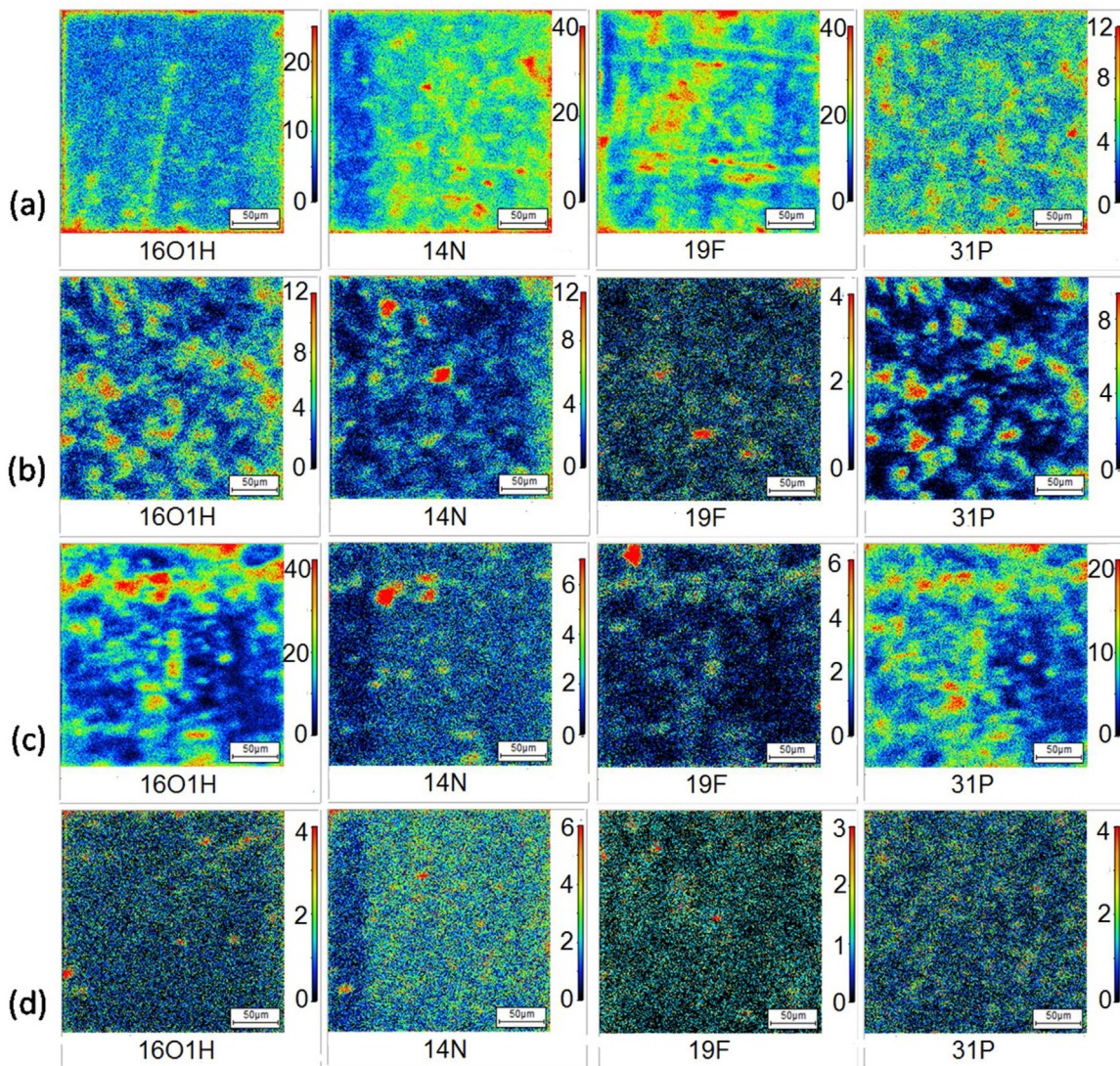


Fig. 1. Surface ion distribution images of $^{16}\text{O}^1\text{H}^+$, $^{14}\text{N}^+$, $^{19}\text{F}^+$ and $^{31}\text{P}^+$ in (a) Virgin (b) HCl treated, (c) H_2SO_4 treated and (d) HNO_3 treated samples. Square region for each element represents the primary beam raster area of $250 \mu\text{m} \times 250 \mu\text{m}$. The color on each pixel for an image corresponds to the counts as shown by the color bar on the right side of the image.

Microscopy (SEM), X-ray photoelectron spectroscopy (XPS), auger electron spectroscopy (AES) etc. provide the surface and depth distribution of various constituent and impurity species which help in understanding the type and nature of chemical attack.

SIMS technique offered various advantages over other surface sensitive techniques (XPS, AES, SEM, EDX (Energy Dispersive X-ray spectroscopy) and RBS (Rutherford Backscattering Spectrometry)) such as the capability to analyze full mass spectrum, very low detection limits (ppm-ppt), 2D (2-dimensional) and 3D (3-Dimensional) distribution analysis of elemental and molecular ionic species, high mass resolution, good lateral resolution (μm) for surface imaging and excellent depth resolution (nm) for depth distribution analysis, direct solid sample analysis, large dynamic range and rapid acquisition of data [7–9]. These numerous advantages offered by SIMS technique have also popularized this technique for investigating the possible corrosion mechanism in different alloys under various corrosive environments. For instance Karar and Singh utilized TOF-SIMS technique to determine the possible chemical corroding agents in the degradation of steel reinforcing bars present inside reinforced concrete structures [10]. Rossi et al. investigated the role of inclusions on the pitting corrosion of austenitic stainless

steel using surface characterization techniques XPS, AES and TOF-SIMS. They have concluded from the surface images obtained using TOF-SIMS technique that no protective (oxide or hydroxide) layer was present on the MnS inclusions and also chlorides are markedly enriched on the MnS inclusions suggesting the pitting corrosion phenomenon [11]. Esmaily et al. employed TOF-SIMS to investigate the corrosion behaviour of Mg alloy AM50 in NaCl induced atmospheric conditions at different temperatures [12]. Seyeux et al. utilized imaging and depth analysis features of SIMS technique to investigate the pitting corrosion mechanism in Al-Cu thin film alloys [13].

Understanding the corrosion process in various materials under different corrosion environments has been mainly carried out using TOF-SIMS, which can be due to its low cost and ease of availability but the better depth profiling capability offered by magnetic sector SIMS due to continuous bombardment of sample surface, has also popularised magnetic sector based SIMS in studying the corrosion process in various alloys. For instance: Cissé et al. utilized Cameca IMS-4F SIMS to investigate the corrosion behaviour of 304L grade stainless steel in high temperature steam and in a simulated Pressurized Water Reactor (PWR) environments [14]. Padhy

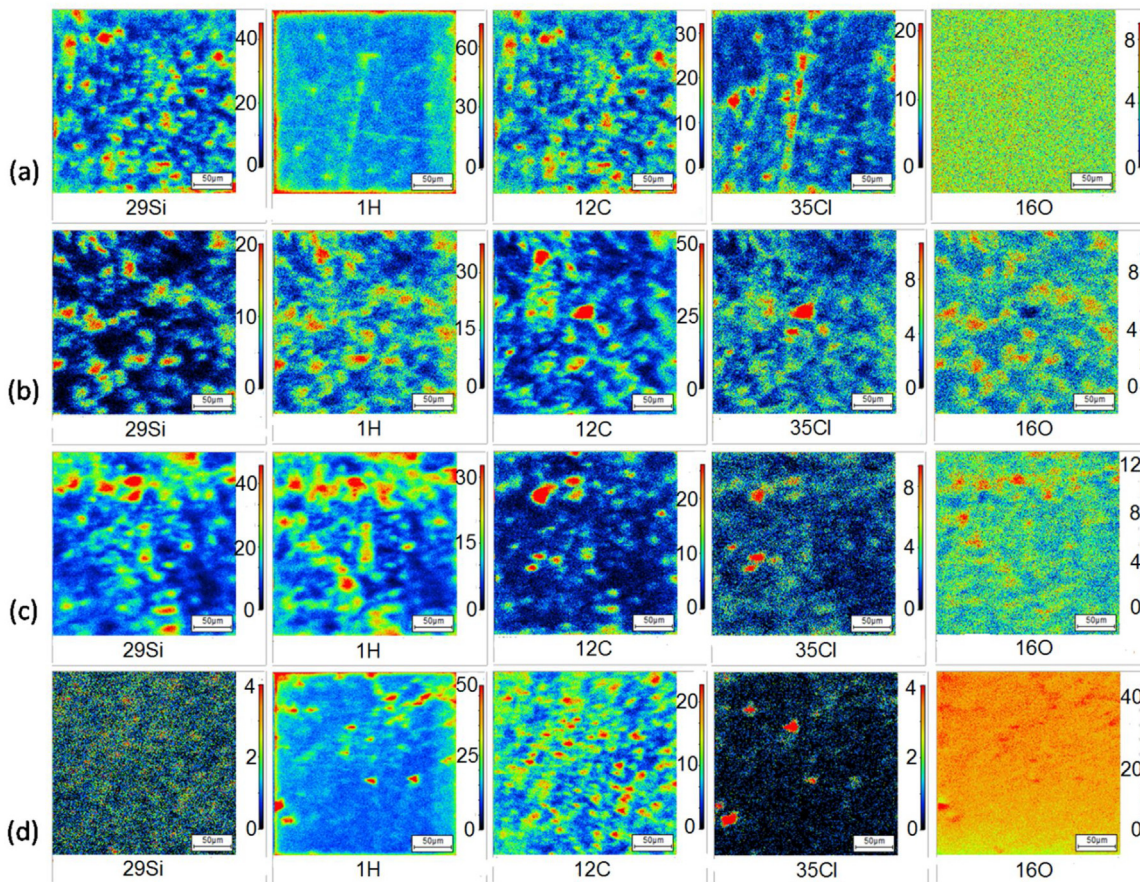


Fig. 2. Surface ion distribution images of $^{29}\text{Si}^+$, $^1\text{H}^+$, $^{12}\text{C}^+$, $^{35}\text{Cl}^+$ and $^{16}\text{O}^+$ in (a) Virgin (b) HCl treated, (c) H_2SO_4 treated and (d) HNO_3 treated samples. Other parameters are same as Fig. 1.

et al. utilized depth analysis feature of Cameca IMS-4F SIMS and other electrochemical techniques to study the effects of nitrogen ion implantation on the corrosion behaviour of 304L stainless steel in 1N HNO_3 solution. They have concluded from SIMS depth profile, the presence of passive layer enriched in chromium nitride and nitrogen which provides corrosion resistance [15]. These studies conclude that through investigations of mass spectra, surface and depth distributions analyses of the elemental and molecular ions, both magnetic sector as well as time of flight based SIMS can provide detailed insights into the type of chemical attack, localised (pitting) corrosion, grain boundary corrosion mechanism and the depth of degradation phenomenon. These reports also suggest that SIMS has extensive potential to investigate the possible corrosion phenomenon in different materials. Despite of these studies, the potentials of SIMS technique alone, in understanding the corrosion mechanism in alloys especially austenitic stainless steel has been much less utilized as compared to other surface sensitive techniques.

The corrosion phenomenon in steel and stainless steel samples under various corrosive environments (H_2SO_4 , HCl, HNO_3 , H_2O_2 , NaCl etc.) has already been reported using chemical, electrochemical as well as various surface analytical techniques other than SIMS. Hence, the aim of present work is to explore the possibility to employ SIMS to study possible corrosion mechanism in austenitic stainless steel due to the effect of HNO_3 , H_2SO_4 and HCl solutions as a corrosive media. Various features offered by SIMS technique such as mass spectra, surface and depth distribution analysis were utilized in investigating the possible mechanism of corrosion. The present work also focuses on providing a suitable methodology using imaging, depth and mass spectra analysis capabilities of SIMS

Table 1
Composition of Type 304 austenitic stainless steel sample used in the present study.

Sample	Elemental concentration (wt%)								
	C	Mn	Si	P	S	Cr	Ni	Fe	N
304 SS	0.05	1.6	0.85	0.04	0.02	18.5	9.5	Bal	0.08

in order to evaluate the type of chemical attack in a particular sample and finding out the root cause of corrosion.

2. Experimental

2.1. Sample preparation

The four samples used in the present studies were made up of Type 304 austenitic stainless steel in sizes of $9\text{ mm} \times 9\text{ mm} \times 1\text{ mm}$. The chemical composition of the sample measured by ICP-MS technique is given in Table 1. Before carrying out the analyses, the samples were mechanically polished in order to achieve micron level surface finish. They were then ultrasonically cleaned with water, ethanol and acetone in order to remove the surface contaminants and then dried. Three of these samples were then completely immersed at the same time in the experimental corrosive media of 10M each of H_2SO_4 , HCl and HNO_3 solutions. They were kept in the solutions for 5 h time period at room temperature. Samples were then removed, washed with water and cleaned with ethanol and acetone and finally dried before SIMS analyses. These samples are designated as Virgin (no treatment), H_2SO_4 treated (subject to 10M H_2SO_4 as the corrosive medium), HNO_3 treated (subject to 10M

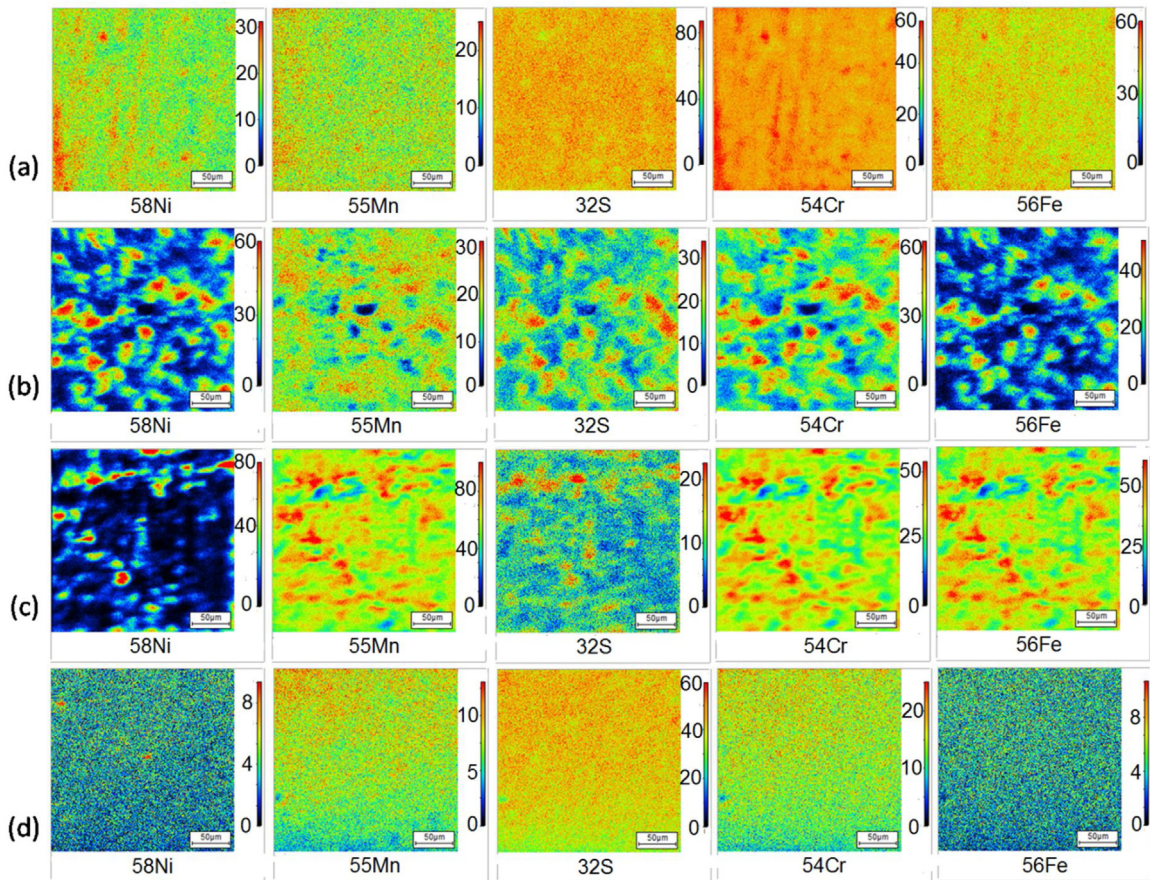


Fig. 3. Surface ion distribution images of $^{58}\text{Ni}^+$, $^{55}\text{Mn}^+$, $^{32}\text{S}^+$, $^{54}\text{Cr}^+$ and $^{56}\text{Fe}^+$ in (a) Virgin (b) HCl treated, (c) H_2SO_4 treated and (d) HNO_3 treated samples. Other parameters are same as Fig. 1.

HNO_3 as a corrosive medium) and HCl treated (subject to 10 M HCl as a corrosive medium).

2.2. SIMS analysis

The surface, depth and mass spectrum analyses in all the four specimens were carried out using magnetic sector based Cameca IMS-7f instrument equipped with both oxygen (O_2^+ and O^-) and cesium (Cs^+) primary ion beams. The surface distribution analyses were carried out using oxygen (O_2^+) primary ion beam at an impact energy of 5 KeV with positive secondary ion detection mode. The lateral resolution primarily depend upon the beam diameter, hence the oxygen beam was tightly focussed to a narrow spot by using various lenses as well as apertures in order to obtain a lateral resolution of $\sim 1 \mu\text{m}$. Primary beam was raster over an area of $250 \mu\text{m} \times 250 \mu\text{m}$ and secondary ions were collected on a high resolution electron multiplier detector having pixel density of 512×512 . Depth distribution analyses were carried out using cesium (Cs^+) primary ion beam at an impact energy of 5 keV in MCs^+ (M being the element of interest) secondary ion detection mode. Primary beam was raster over an area of $250 \mu\text{m} \times 250 \mu\text{m}$ and secondary ions were collected over an analysis region of $62.5 \mu\text{m}$ in diameter at the centre of raster area in order to remove the crater edge effects. Mass spectral analyses from 1 amu to 200 amu were also acquired using both oxygen (O_2^+) and cesium (Cs^+) primary ion beam in positive and negative secondary ion detection modes respectively.

3. Results and discussion

3.1. Surface distribution analysis

Figs. 1 and 2 show the surface ion distribution of various elements (alloying and impurities) in (a) Virgin, (b) HCl treated, (c) H_2SO_4 treated and (d) HNO_3 treated samples. The elements N, F, P, Si, H, C and Cl were non-homogenously distributed in Virgin, HCl treated and H_2SO_4 treated samples. Similar non-homogenous distributions of elements such as C and Si were also found in high alloy stainless steel sample analyzed by SIMS in our previous study [16]. Also, it is clearly visible from the figures that the size of precipitates is larger in HCl and H_2SO_4 treated samples compared to the Virgin sample which is due to the formation of a corroded layer and its morphology. The size of precipitates in virgin and HNO_3 treated samples were in the range of $8 \mu\text{m}$ – $12 \mu\text{m}$ while it increases to $25 \mu\text{m}$ in case of HCl and H_2SO_4 treated samples. Fig. 3 represents the surface ion distribution images of the alloying elements Ni, Mn, S, Cr and Fe in the same set of samples. Uniform surface distribution of these elements were observed in case of virgin and HNO_3 treated samples whereas in case of HCl treated as well as H_2SO_4 treated samples, the distribution of these elements were non-uniform which can also be due to the formation of the corroded layer in the sample surface and its morphology. The change in surface morphology in case of HCl treated mild steel sample compared to untreated sample has also been reported by Noor and Moubaraki but they have not provided any detailed information on the distribution of the elements in corroded surface [5]. Similar modification in surface morphology for Type 304 austenitic stainless steel under 2 M and 5 M H_2SO_4 acid environments has also been

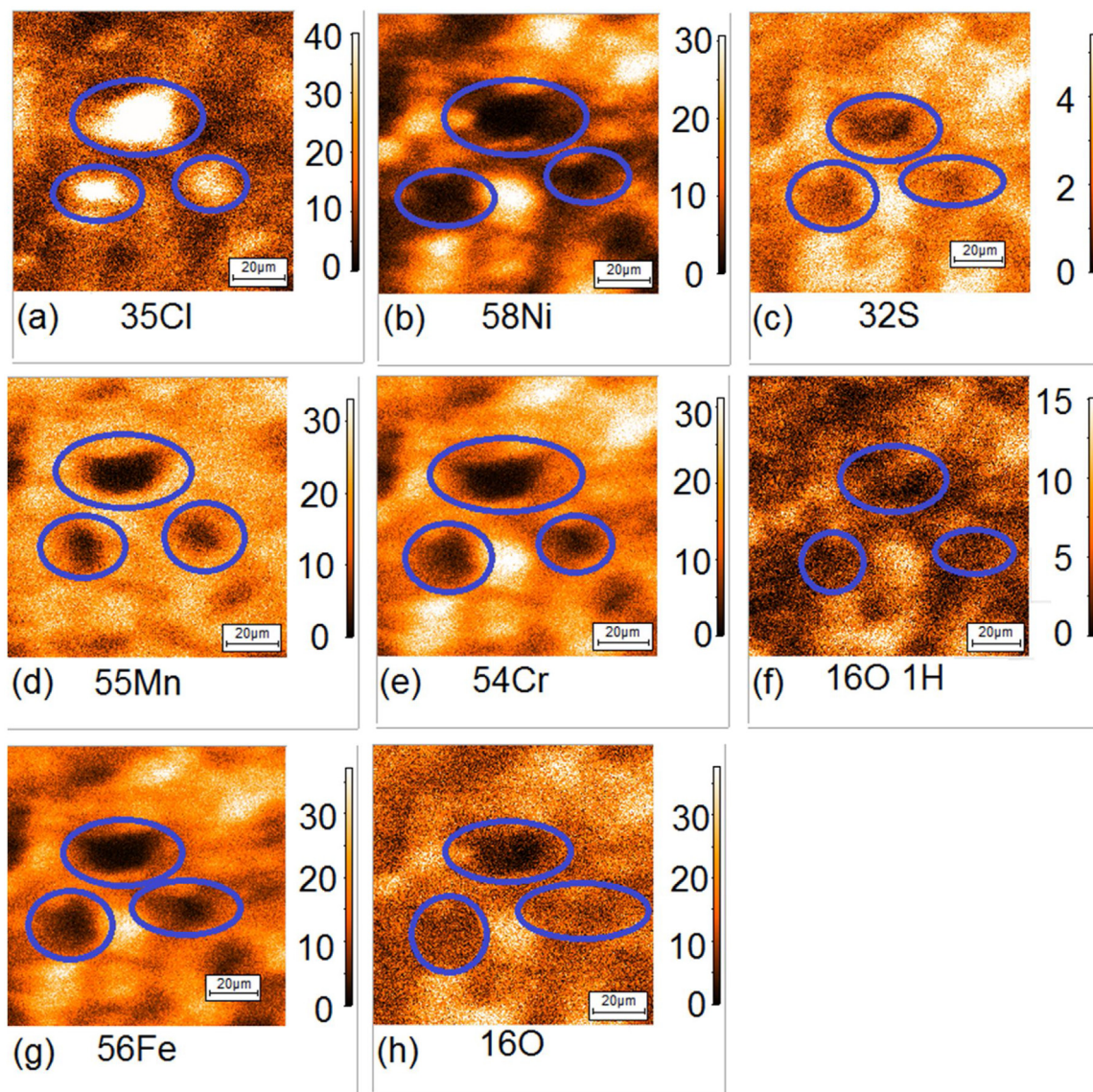


Fig. 4. Magnified surface ion distribution images of (a) $^{35}\text{Cl}^+$, (b) $^{58}\text{Ni}^+$, (c) $^{32}\text{S}^+$, (d) $^{55}\text{Mn}^+$, (e) $^{54}\text{Cr}^+$, (f) $^{16}\text{O}^1\text{H}^+$, (g) $^{56}\text{Fe}^+$ and (h) $^{16}\text{O}^+$ in HCl treated sample. Regions of Cl enrichment and depletion of Ni, S, Mn, Cr, OH, Fe and O are circled for clarity. The color on each pixel for an image corresponds to the counts as shown by the color bar on the right side of the image.

reported by Loto et al. using Scanning Electron Microscopy (SEM) but they also have not provided any information regarding the distribution of various elements in these corroded surfaces [17]. It is evident from the figures that the surface distribution of all the alloying elements (Cr, Mn, Ni, Fe, S) as well as oxygen in the virgin and the HNO_3 treated samples are quite similar and are also homogeneously distributed which concluded that HNO_3 treated specimen have least modification in surface morphology. A comparison of surface distribution of impurity ions (N, F, Cl and P) in Virgin and HNO_3 treated specimens also concludes that the distributions of these elements are more homogenous in HNO_3 treated specimen compared to Virgin sample. This observation indicates that HNO_3 doesn't corrode the specimen although it has removed or dissolved the surface impurities.

In order to investigate the surface corrosion mechanism in HCl treated sample, interpretation of surface distribution of various elements are important. The local magnified surface images of (a) $^{35}\text{Cl}^+$, (b) $^{58}\text{Ni}^+$, (c) $^{32}\text{S}^+$, (d) $^{55}\text{Mn}^+$, (e) $^{54}\text{Cr}^+$, (f) $^{16}\text{O}^1\text{H}^+$, (g) $^{56}\text{Fe}^+$ and (h) $^{16}\text{O}^+$ are shown in Fig. 4. It can be concluded from visualising the figure that the region with a high chlorine presence

shows a depletion of not only the constituent elements i.e. Fe, Ni, Cr, Mn and S but even for elements like oxygen and molecular species OH, suggesting the localised attack or pitting corrosion on stainless steel surface by the chloride solution. Similar surface ion distribution pattern of these elements acquired at a different location is shown in Fig. 5 with higher magnification as compared to Fig. 4. The pitting behaviour of Type 304 stainless steel in HCl solution can be correlated with the presence and composition of non-metallic inclusions like C and Cl (Figs. 2b, 4 and 5). No oxide or hydroxide species was observed on these localized non-metallic inclusions and therefore function as a nucleation sites for pit initiation in chloride-containing solutions. The pitting corrosion phenomenon on stainless steel surface exposed to FeCl_3 solutions was also observed by Rossi et al. but the pitting nucleation sites were non metallic inclusions of MnS [11].

In case of H_2SO_4 treated sample, a different surface distribution of elemental and molecular ionic species on the sample surface was observed compared to HCl treated sample (Figs. 1c, 2c and 3c). The group of elements O, H, C, Si, Cl, S and molecular species OH have similar surface distribution patterns suggesting that the attack

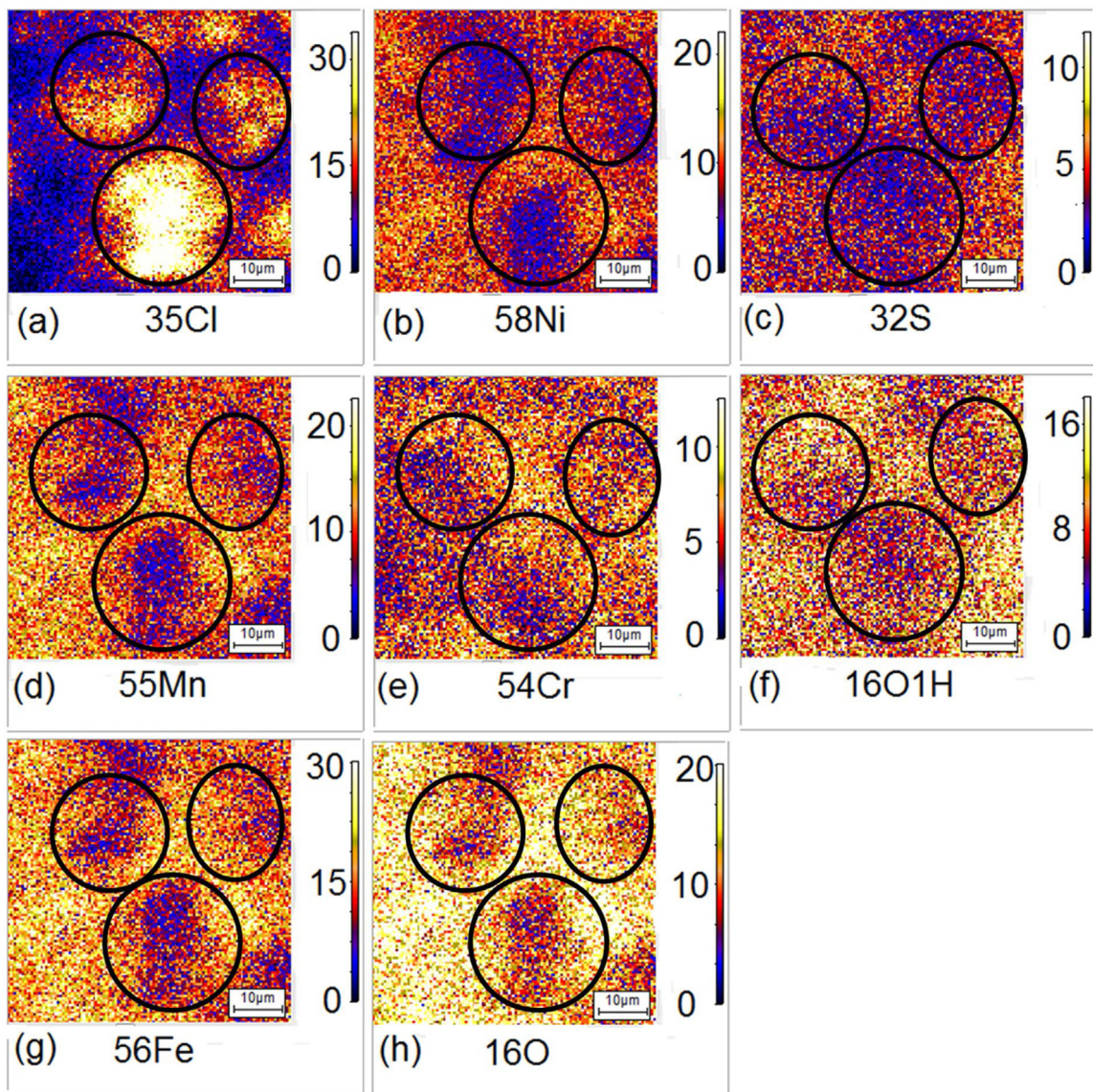


Fig. 5. Magnified surface ion distribution images of (a) $^{35}\text{Cl}^+$, (b) $^{58}\text{Ni}^+$, (c) $^{32}\text{S}^+$, (d) $^{55}\text{Mn}^+$, (e) $^{54}\text{Cr}^+$, (f) $^{16}\text{O}^1\text{H}^+$, (g) $^{56}\text{Fe}^+$ and (h) $^{16}\text{O}^+$ acquired at different location in HCl treated sample. Regions of Cl enrichment and depletion of Ni, S, Mn, Cr, OH, Fe and O are circled for clarity. The color on each pixel for an image corresponds to the counts as shown by the color bar on the right side of the image.

of sulfur species are associated with the formation of oxides and hydroxides of other elements while the group of alloying elements Ni, Mn, Cr and Fe have similar distribution patterns.

3.2. Depth distribution analysis

It has been widely reported that detection of MC_n⁺ secondary molecular ions (M being the element of interest) as compared to the detection of respective atomic secondary ions results in a pronounced reduction of matrix effects [18]. Hence, this approach was used in the present study to investigate the depth distribution analyses of elements Cr, Ni, Mn and Fe in the samples. Fig. 6(a)–(d) shows the depth distribution analyses of alloying elements Cr, Ni, Mn and Fe respectively in the Virgin, HCl treated, H_2SO_4 treated and HNO_3 treated samples. The depth distribution curves revealed that the abundance of Cr, Ni, Mn and Fe are least at the surface (upto 2000 s) for H_2SO_4 treated samples as compared to virgin, HCl treated and HNO_3 treated samples. Similar trend has also been reported for Cr, Ni and Fe in 2 M H_2SO_4 treated sample surface in

Type 304 austenitic stainless steel sample compared to untreated sample using Energy Dispersive Spectrometer analysis by Loto et al. [17]. A very distinctive feature in case of HNO_3 treated sample has been observed as shown in Fig. 6 for alloying elements Cr, Ni, Mn and Fe. As it is evident from the figure, a peak has been observed for these elements at the surface upto 2000 s. Also, there is an appearance of a trough region starting from 2000 s and expand upto 6500 s which also confirms that the elements from within region have diffused to surface region upto 2000 s and form a passive layer enriched in alloying elements especially Cr and Ni which are known to have corrosion resistance property and hence this passive layer has slowed down or stopped the corrosion process. The formation of passive layer enriched in Cr, and Ni at the surface of 304 stainless steel sample has also been reported by Molchan et al. but the samples were immersed in pyrrolidinium-2-one trifluoroacetate ionic liquid [19]. These results conclude that the corrosion is inhibited in case of HNO_3 treated sample under the experimental corrosive environmental parameters which has also been supported by the surface ion distribution images as shown in Figs. 1d, 2d and 3d (sim-

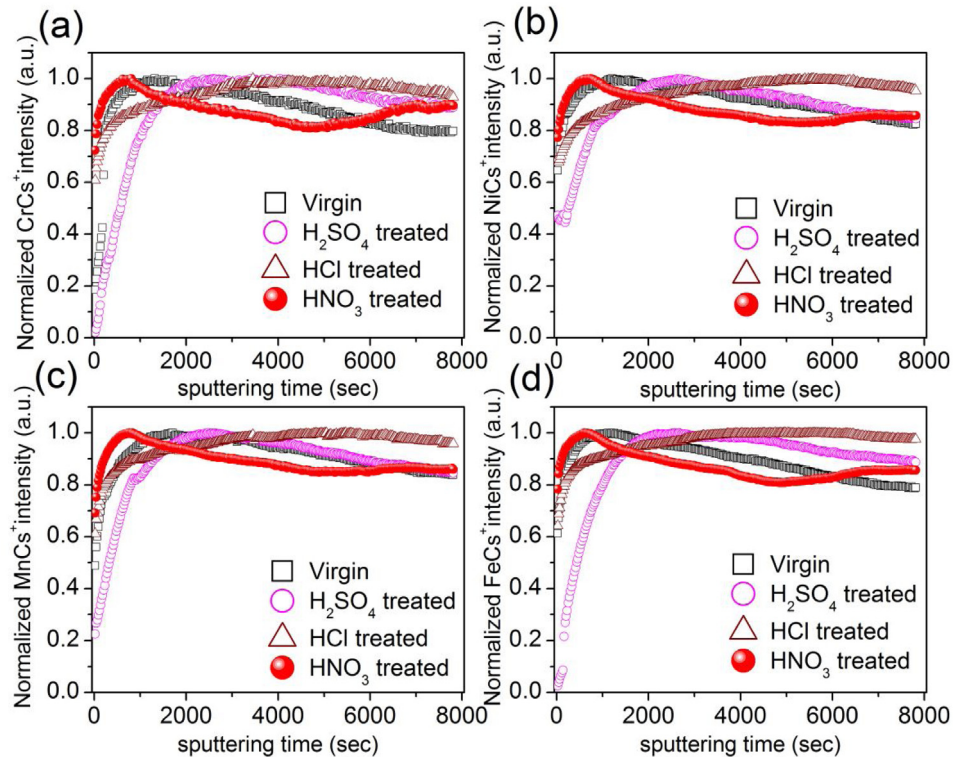


Fig. 6. SIMS depth profiles of (a) Cr, (b) Ni, (c) Mn and (d) Fe in Virgin, H₂SO₄ treated, HCl treated and HNO₃ treated samples employing MCs⁺ (where M being the element of interest) secondary ion monitoring approach.

ilar homogenous distribution patterns for all the alloying elements in case of virgin and HNO₃ treated sample).

The depth profiles of elemental and molecular ions O, OH, H, S and Cl using MCs⁺ approach are shown in Fig. 7(a), (b), (c), (d) and (e), respectively. As it is evident from the figures, the concentration of O, OH and H are highest in case of H₂SO₄ followed by HCl treated sample. This also indicated that the concentration of oxides as well as hydroxide containing species are higher in the corroded surface in case of H₂SO₄ treated sample followed by HCl treated sample. The S and Cl concentrations are higher in H₂SO₄ and HCl treated specimens, respectively (Fig. 7(d) and (e)) which represents the attack of sulfur containing species in H₂SO₄ and chloride containing species in HCl treated samples. Similar trend for sulfur has also been reported by Loto et al. for H₂SO₄ treated specimen Type 304 stainless steel compared to untreated sample analyzed by Energy Dispersive Spectrometer [17]. These analyses also indicated that a comparison of the depth distribution curves of elemental or molecular ions in virgin sample and corroded sample provides a detailed insight of the type and depth of chemical attack. Another important feature that has also been observed from these depth profiles is that, in all the cases the distribution profiles of elements and molecular ions are quite similar for virgin and for HNO₃ treated samples. This also confirms that HNO₃ is less corrosive as compared to H₂SO₄ and HCl under the experimental corrosive environmental parameters. Since the distribution of O and OH species in the virgin and HNO₃ treated sample are not clearly visible in Fig. 7a and b, Fig. 8 is shown separately for the distribution of these species in virgin and HNO₃ treated sample. The distribution profiles shown in Fig. 8 conclude that oxide and hydroxide species in surface layer are higher in HNO₃ treated sample compared to virgin sample. Hence, by observing the depth profiles shown in Figs. 6 and 8 one may conclude that a passive layer enriched in Cr, Ni, Mn, Fe, O and OH has been formed on the surface of HNO₃ treated sample.

3.3. Mass spectra analysis

3.3.1. Intensity variations of oxides and hydroxides containing species

Mass spectra analysis from 1 amu to 200 amu has been carried out using O₂⁺ and Cs⁺ primary ion beam in positive and negative secondary ion detection modes respectively. Fig. 9 represents the intensity variations of various oxides and hydroxides containing species. It can be concluded from the figures that the oxides and hydroxides containing species are higher in intensity for H₂SO₄ treated sample followed by HCl treated sample. It is also apparent from the figures that the intensity variations for these ions in case of virgin and HNO₃ treated samples are similar which also confirms that a very minimal surface modifications has taken place in case of HNO₃ treated sample. These analyses also substantiate the fact that the HNO₃ is least corrosive for Type 304 austenitic stainless steel under the experimental corrosive conditions.

3.3.2. Intensity variations of sulfur containing species

Fig. 10(a) and (b) represents the intensity variations of various sulfur containing species in virgin, H₂SO₄ treated, HCl treated and HNO₃ treated samples. It is apparent from the figures that the sulfur as well as the sulfur containing oxide species are higher in concentration in H₂SO₄ treated samples. This also confirms that the corrosive layer is formed by the attack of sulfur species and the corrosive layer is enriched in sulfur and sulfur containing oxide and hydroxides species. Hence, monitoring of these elemental and molecular ions using mass spectra analysis feature of SIMS can be used to identify the attack of sulphur species in a corroded specimen.

3.3.3. Intensity variations of chlorine containing species

Fig. 11 represents the intensity variations of various chloride containing species in virgin, H₂SO₄ treated, HCl treated and HNO₃

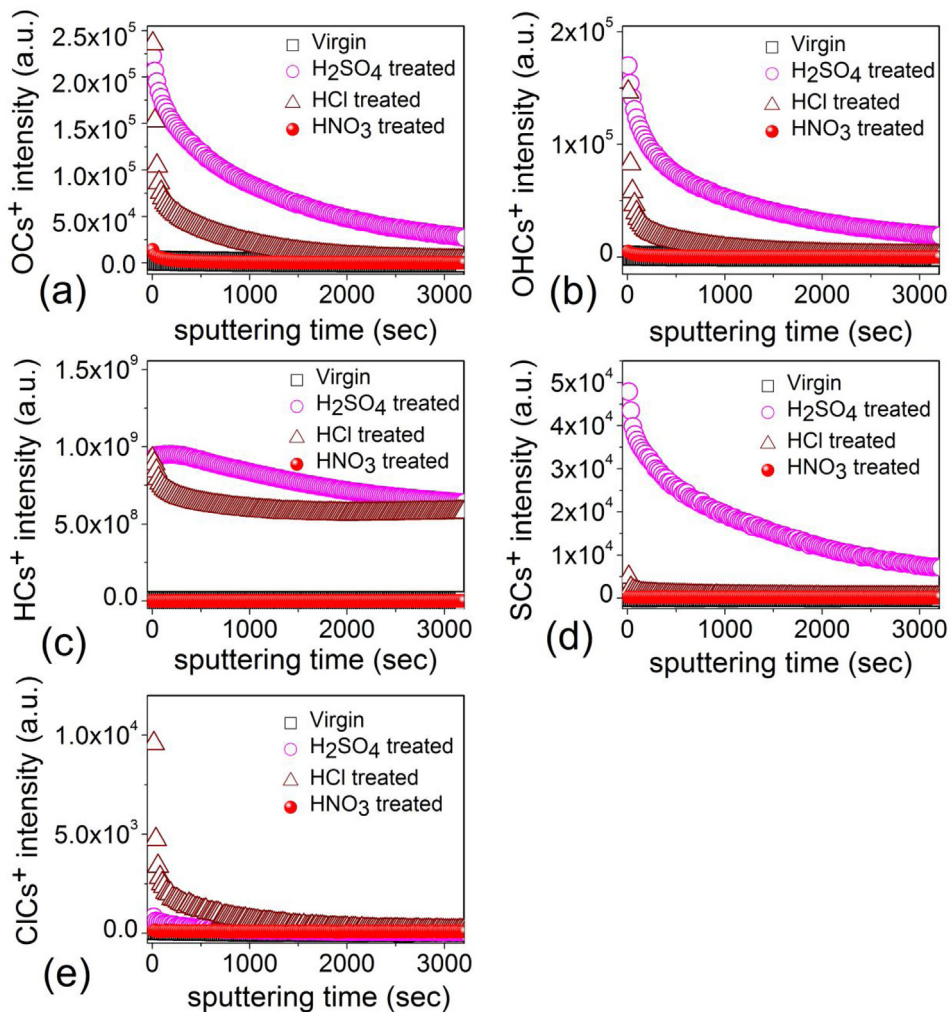


Fig. 7. SIMS depth profiles of (a) O, (b) OH, (c) H, (d) S and (e) Cl in Virgin, H_2SO_4 treated, HCl treated and HNO_3 treated samples using MCs^+ (where M being the element of interest) secondary ion monitoring approach.

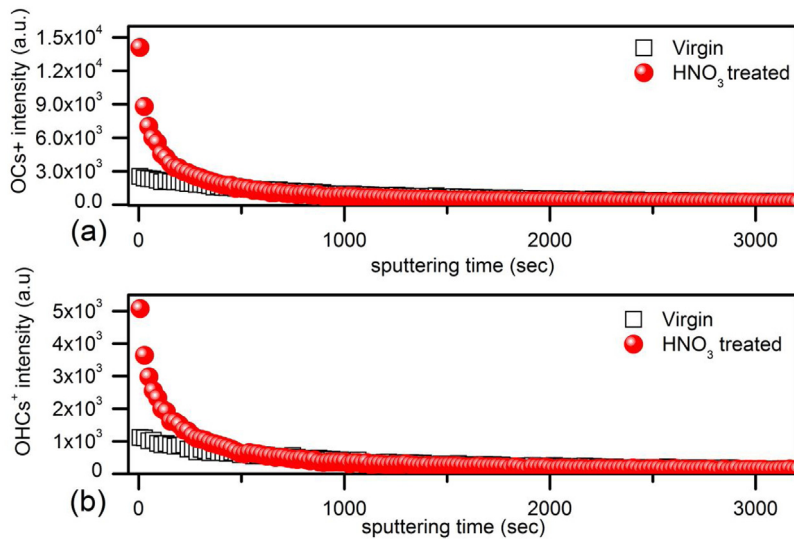


Fig. 8. SIMS depth profiles of (a) O and (b) OH in Virgin and HNO_3 treated sample using MCs^+ (where M being the element of interest) secondary ion monitoring approach.

treated samples. It can be concluded from the figure that the chlorine and chlorine containing species are higher in concentration in HCl treated samples. This also confirms that the corrosive layer

is formed by the attack of chloride ions and the corrosive layer is enriched in the chlorine and associated species. Similarly, monitoring of these elemental and molecular ions using mass spectra

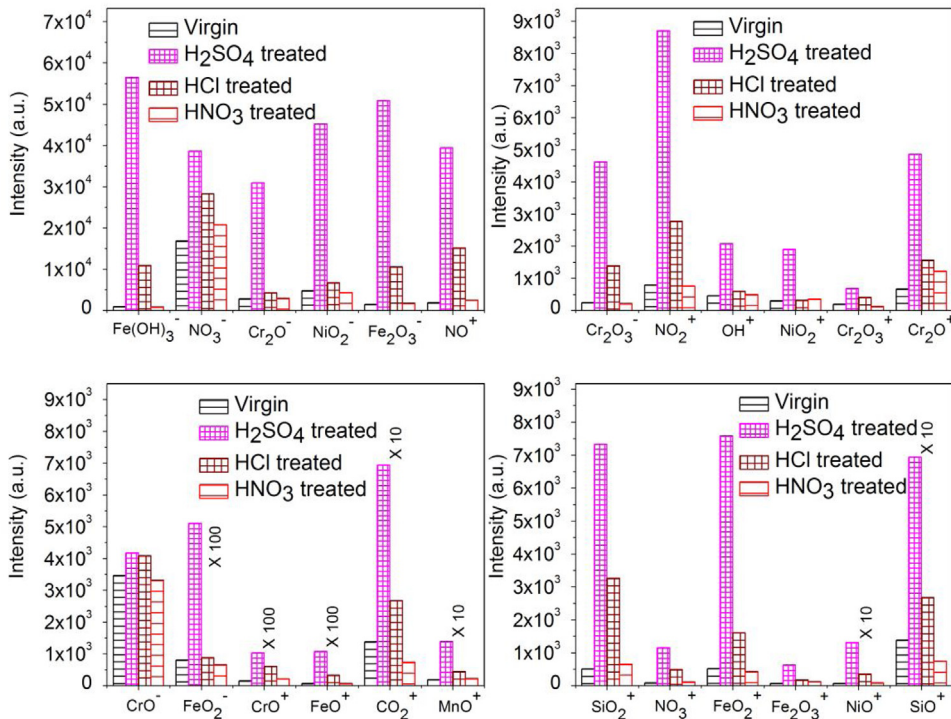


Fig. 9. Intensity variation of various oxides and hydroxides containing ions in Virgin, H_2SO_4 treated, HCl treated and HNO_3 treated samples. The intensity of each ion has been obtained from the integrated area under the corresponding mass peak curve.

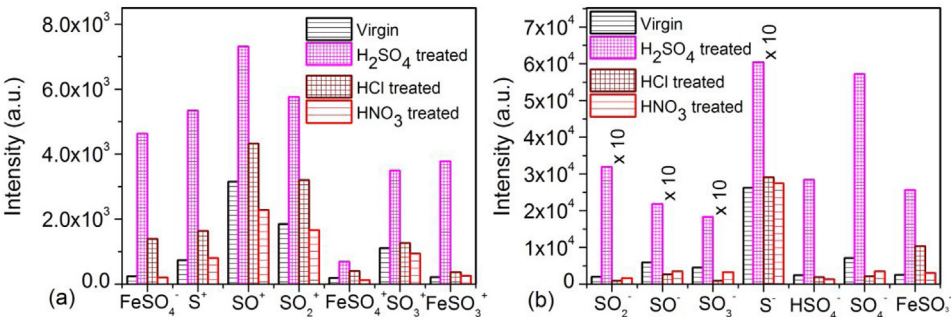


Fig. 10. Intensity variation of various sulfur containing ions in Virgin, H_2SO_4 treated, HCl treated and HNO_3 treated samples. The intensity of each ion has been obtained from the integrated area under the mass peak curve.

analysis feature of SIMS can be used to identify the attack of chloride species in a corroded specimen.

3.3.4. Intensity variations of nitrogen containing species

Fig. 12 represents the intensity variations of various nitrogen containing species in virgin, and HNO_3 treated samples. A very different trend in the variation of nitrogen and nitrogen containing oxide species has been observed from Fig. 12 as compared to H_2SO_4 and HCl treated samples for sulfur and chlorine containing species respectively. The variation of N^+ , NO_2^+ and NO_3^- ionic species are almost similar in virgin and HNO_3 treated samples indicating no surface corrosion process due to nitrogen species. While the intensity of some of the ionic oxide species such as NO^- , NO^+ , NO_3^- and NO_3^+ are higher in HNO_3 treated sample compared to virgin sample confirming the presence of passive layer in HNO_3 treated sample.

3.3.5. Intensity variations of impurity elemental and molecular species

Fig. 13 represents the intensity variations of various impurities F, Mg, Ca, C (mainly surface carbon) and associated molecular ions in

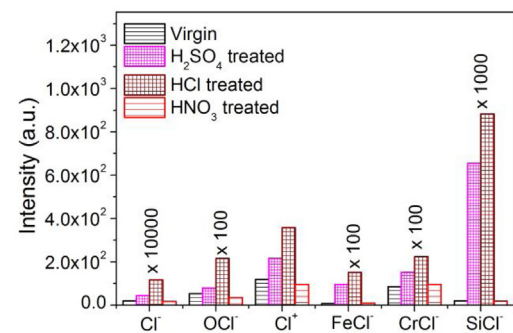


Fig. 11. Intensity variation of various chlorine containing ions in Virgin, H_2SO_4 treated, HCl treated and HNO_3 treated samples. The intensity of each ion has been obtained from the integrated area under the corresponding mass peak curve.

virgin, H_2SO_4 treated, HCl treated and HNO_3 treated samples. It can be observed from the figure that the surface is highly contaminated in case of virgin sample followed by HNO_3 treated sample. It can be seen from the figure that the HNO_3 treated sample has very

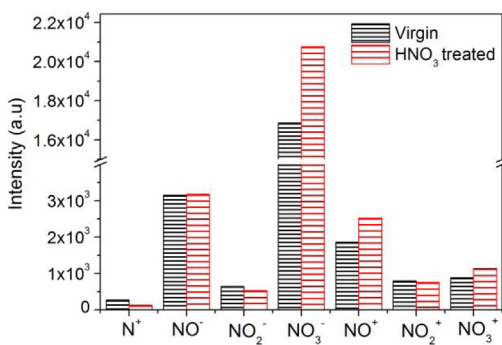


Fig. 12. Intensity variation of various nitrogen and nitrogen containing ions in Virgin and HNO₃ treated sample. The intensity of each ion has been obtained from the integrated area under the corresponding mass peak curve.

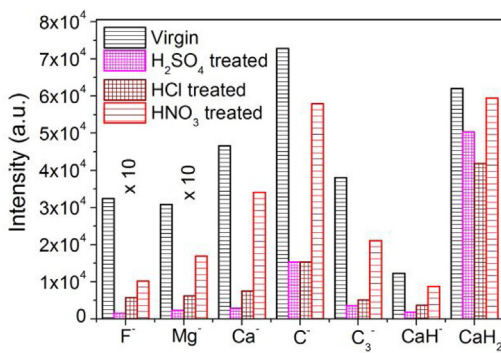


Fig. 13. Intensity variation of various impurities containing elemental and molecular ions in Virgin, H₂SO₄ treated, HCl treated and HNO₃ treated samples. The intensity of each ion has been obtained from the integrated area under the mass peak curve.

small surface modifications (mainly associated with the removal of surface impurities) compared to the HCl and H₂SO₄ treated sample under the experimental corrosive environments. This observation further corroborates HNO₃ is less corrosive in comparison to HCl and H₂SO₄ acids.

4. Summary and conclusions

SIMS technique has been used to investigate the corrosion mechanism in Type 304 austenitic stainless steel under the effect of corrosive environments of 10 M each of H₂SO₄, HCl and HNO₃ solutions. Surface distribution analysis revealed that the elements N, F, P, Si, H, C and Cl were non-homogenously distributed in Virgin, HCl treated and H₂SO₄ treated samples. In addition, the size of these precipitates are larger (8 μm–25 μm) in HCl and H₂SO₄ treated samples compared to the virgin sample (8 μm–12 μm) which can be due to the formation of corrosive layer and its morphology. The surface distribution patterns of alloying elements S, Cr, Mn, Fe and Ni are homogenous in case of Virgin and HNO₃ treated samples while the distribution patterns becomes non-homogenous in case of H₂SO₄ and HCl treated sample. Interpretation of surface ion distribution images concluded localised or pitting corrosion phenomenon in case of HCl treated specimen. Depth distribution and mass spectra analyses revealed that in case of H₂SO₄ and HCl treated samples, the surface layer was enriched in oxide and hydroxide containing ions and the concentration of these ions were higher in case of H₂SO₄ followed by HCl treated specimen. Mass spectrum analysis also revealed that the concentration of sulfur and chlorine containing ions were higher in H₂SO₄ treated and HCl treated samples, respectively and thereby indicating the corrosion

associated with these types of species. Depth distribution analysis of alloying elements Cr, Mn, Ni and Fe revealed that there was a formation of passive layer in case of HNO₃ treated specimens, which has inhibited the corrosion process. The study shows that surface imaging, depth distribution and mass spectrum analysis features of SIMS technique can be utilized for understanding the possible corrosion mechanism in different kinds of alloys.

Acknowledgments

The authors gratefully acknowledge Dr. P. G. Jaison, Dr. Pranaw Kumar and Mr. Vijay M. Telmore for the experimental support and their valuable suggestions for the improvement of the manuscript. The authors are thankful to Dr. Arnab Sarkar, Dr. S. Kannan, Head, Fuel Chemistry Division, Prof. B.S. Tomar, Director, Radiochemistry and Isotope Group, B.A.R.C. for their constant support and encouragement in SIMS related work.

References

- [1] K.H. Lo, C.H. Shek, J.K.L. Lai, Recent developments in stainless steels, Mater. Sci. Eng. R 65 (2009) 39–104.
- [2] S. Şahin, M. Übeyli, A review on the potential use of austenitic stainless steels in nuclear fusion reactors, J. Fusion Energy 27 (2008) 271–277.
- [3] M. Talha, C.K. Behera, O.P. Sinha, A review on nickel-free nitrogen containing austenitic stainless steels for biomedical applications, Mater. Sci. Eng. C 33 (2013) 3563–3575.
- [4] E.E. Rees, D.S. McPhail, M.P. Ryan, J. Kelly, M.G. Dowsett, Low energy SIMS characterisation of ultra thin oxides on ferrous alloys, Appl. Surf. Sci. 203–204 (2003) 660–664.
- [5] E.A. Noor, A.H.A. Moubaraki, Corrosion behavior of mild steel in hydrochloric acid solutions, Int. J. Electrochem. Sci. 3 (2008) 806–818.
- [6] I. Illyas, D.S. Yawas, S.Y. Aku, Corrosion behavior of austenitic stainless steel in sulphuric acid at various concentrations, Adv. Appl. Sci. Res. 3 (6) (2012) 3909–3915.
- [7] A. Benninghoven, F.G. Rüdenauer, H.W. Werner, Secondary Ion Mass Spectrometry: Basic Concepts, Instrumental Aspects, Applications, and Trends, Wiley, 1987.
- [8] R.G. Wilson, F.A. Stevie, C.W. Magee, Secondary Ion Mass Spectrometry: A Practical Handbook for Depth Profiling and Bulk Impurity Analysis, Wiley, New York, 1989.
- [9] D.S. Mcphail, Applications of secondary ion mass spectrometry (SIMS) in materials science, J. Mater. Sci. 41 (2006) 873–903.
- [10] N. Karar, S.K. Singh, Understanding corrosion in steel reinforced concrete structures: a limited study using ToF-SIMS, Vacuum 121 (2015) 5–8.
- [11] A. Rossi, B. Elsener, G. Hähner, M. Textor, N.D. Spencer, XPS, AES and ToF-SIMS investigation of surface films and the role of inclusions on pitting corrosion in austenitic stainless steels, Surf. Interface Anal. 29 (2000) 460–467.
- [12] M. Esmaily, P. Malmberg, M. Shahabi-Navid, J.E. Svensson, L.G. Johansson, A ToF-SIMS investigation of the corrosion behavior of Mg alloy AM50 in atmospheric environments, Appl. Surf. Sci. 360 (2016) 98–106.
- [13] A. Seyeux, G.S. Frankel, N. Misset, K.A. Unocic, L.H. Klein, A. Galtayries, P. Marcus, ToF-SIMS imaging study of the early stages of corrosion in Al-Cu thin films, J. Electrochem. Soc. 158 (6) (2011) C165–C171.
- [14] Sarata Cissé, Lydia Laffont, Benoit Tanguy, Marie-Christine Lafont, Eric Andrieu, Effect of surface preparation on the corrosion of austenitic stainless steel 304L in high temperature steam and simulated PWR primary water, Corros. Sci. 56 (2012) 209–216.
- [15] N. Padhy, S. Ninghsen, B.K. Panigrahi, U. Kamachi Mudali, Corrosion behaviour of nitrogen ion implanted AISI type 304L stainless steel in nitric acid medium, Corros. Sci. 52 (2010) 104–112.
- [16] V. Karki, D. Alamelu, Surface and depth distribution of components in high alloy stainless steel using secondary ion mass spectrometry, Int. J. Mass Spectrom. 407 (2016) 101–105.
- [17] R.T. Loto, C.A. Loto, A.P.I. Popoola, M. Ranyaoa, Corrosion resistance of austenitic stainless steel in sulphuric acid, Int. J. Phys. Sci. 7 (10) (2012) 1677–1688.
- [18] K. Wittmaack, Mechanism of MCs+ formation in Cs based secondary ion mass spectrometry, Appl. Surf. Sci. 606 (2012) L18–L21.
- [19] I.S. Molchan, G.E. Thompson, J. Walton, P. Skeldon, A. Tempez, S. Legendre, Passivation behaviour of 304 stainless steel in an ionic liquid with a fluorinated anion, Appl. Surf. Sci. 357 (2015) 37–44.